

## Research paper

# Seno-destructive smooth muscle cells in the ascending aorta of patients with bicuspid aortic valve disease



Brittany Balint<sup>a,b</sup>, Hao Yin<sup>a</sup>, Zengxuan Nong<sup>a</sup>, John-Michael Arpino<sup>a,b</sup>, Caroline O'Neil<sup>a</sup>, Stephanie R. Rogers<sup>a</sup>, Varinder K. Randhawa<sup>c</sup>, Stephanie A. Fox<sup>d,e</sup>, Jacqueline Chevalier<sup>a,b</sup>, Jason J. Lee<sup>a,b</sup>, Michael W.A. Chu<sup>d,e</sup>, J. Geoffrey Pickering<sup>a,b,c,e,f,\*</sup>

<sup>a</sup> Roberts Research Institute, The University of Western Ontario, 1151 Richmond St. N., London, ON N6A 5B7, Canada

<sup>b</sup> Department of Medical Biophysics, The University of Western Ontario, 1151 Richmond St. N., London, ON N6A 5C1, Canada

<sup>c</sup> Departments of Medicine (Cardiology), The University of Western Ontario, 1151 Richmond St. N., London, ON N6A 5C1, Canada

<sup>d</sup> Department of Surgery, The University of Western Ontario, 1151 Richmond St. N., London, ON N6A 5C1, Canada

<sup>e</sup> London Health Sciences Centre, 339 Windermere Rd., London, ON N6A 5A5, Canada

<sup>f</sup> Department of Biochemistry, The University of Western Ontario, 1151 Richmond St. N., London, ON N6A 5C1, Canada

## ARTICLE INFO

## Article history:

Received 12 March 2019

Received in revised form 22 April 2019

Accepted 30 April 2019

Available online 9 May 2019

## Keywords:

Bicuspid aortic valve

Aortic aneurysm

Smooth muscle cells

Cellular senescence

Collagenase

## ABSTRACT

**Background:** Ascending aortic aneurysms constitute an important hazard for individuals with a bicuspid aortic valve (BAV). However, the processes that degrade the aortic wall in BAV disease remain poorly understood.

**Methods:** We undertook in situ analysis of ascending aortas from 68 patients, seeking potentially damaging cellular senescence cascades. Aortas were assessed for senescence-associated- $\beta$ -galactosidase activity, p16<sup>Ink4a</sup> and p21 expression, and double-strand DNA breaks. The senescence-associated secretory phenotype (SASP) of cultured-aged BAV aortic smooth muscle cells (SMCs) was evaluated by transcript profiling and consequences probed by combined immunofluorescence and circular polarization microscopy. The contribution of p38 MAPK signaling was assessed by immunostaining and blocking strategies.

**Findings:** We uncovered SMCs at varying depths of cellular senescence within BAV- and tricuspid aortic valve (TAV)-associated aortic aneurysms. Senescent SMCs were also abundant in non-aneurysmal BAV aortas but not in non-aneurysmal TAV aortas. Multivariable analysis revealed that BAV disease independently associated with SMC senescence. Furthermore, SMC senescence was heightened at the convexity of aortas associated with right-left coronary cusp fusion. Aged BAV SMCs had a pronounced collagenolytic SASP. Moreover, senescent SMCs in the aortic wall were enriched with surface-localized MMP1 and surrounded by weakly birefringent collagen fibrils. The senescent-collagenolytic SMC phenotype depended on p38 MAPK signaling, which was chronically activated in BAV aortas.

**Interpretation:** We have identified a cellular senescence-collagen destruction axis in at-risk ascending aortas. This novel "seno-destructive" SMC phenotype could open new opportunities for managing BAV aortopathy.

**Fund:** Canadian Institutes of Health Research, Lawson Health Research Institute, Heart and Stroke Foundation of Ontario/Barnett-Ivey Chair.

© 2019 The Authors. Published by Elsevier B.V. This is an open access article under the CC BY-NC-ND license (<http://creativecommons.org/licenses/by-nc-nd/4.0/>).

## 1. Introduction

Individuals with a bicuspid aortic valve (BAV) are at risk of developing ascending aortic aneurysms [1]. The basis of these aneurysms, and their complications of dissection and rupture, are incompletely understood but hemodynamic and genetic factors are implicated [2–4]. There are well-recognized pathological features of BAV aortopathy,

including elastin fiber degradation, non-inflammatory loss of smooth muscle cells (SMCs), and accumulation of mucoid extracellular matrix (ECM) [5]. However, there are currently no strategies to prevent or delay aortic degeneration in individuals with a BAV and a better understanding of the cellular events that underlie the destructive process is warranted.

Medial SMCs are central to aortic structure and function. SMCs impart stability to the aorta through their contractile properties, their ability to secrete and assemble ECM fibrils [6–8], and by the firm attachments they form with each other and the ECM [9,10]. Inherently abnormal SMCs can render the aortic wall susceptible to dilation and

\* Corresponding author at: London Health Sciences Centre, 339 Windermere Rd., London, ON N6A 5A5, Canada.

E-mail address: [gpickering@roberts.ca](mailto:gpickering@roberts.ca) (J.G. Pickering).

**Research in context***Evidence before this study*

Individuals with a bicuspid aortic valve (BAV) are prone to developing ascending aortic aneurysms, which can catastrophically rupture or dissect. The integrity of the aortic wall is determined in large part by the actions of smooth muscle cells (SMCs), including their contractile and synthetic properties. SMC apoptosis and differentiation defects have been identified in BAV aortas yet the basis for the profound degenerative changes in the aortic wall remains poorly understood.

*Added value of this study*

We discovered senescent SMCs in the media of dilated thoracic aortas, and found a particular predisposition to SMC senescence in BAV aortopathy. Moreover, we determined that these prematurely aged SMCs have a destructive senescence-associated secretory phenotype (SASP). This SASP entails reduced expression of fibrillar collagens and upregulated collagenases, including membrane-localized MMP1. Associated with this was local collagen fibril degradation within the aortic media. This senescent and destructive cellular phenotype was particularly enriched at sites of hemodynamic perturbation and is controlled by p38 MAPK.

*Implications of all the available evidence*

The presence of “seno-destructive” SMCs in the BAV aortic wall reveals a mechanistic route to aortic degeneration in individuals with BAV and opens a new, senescence-targeting framework for potential therapy.

dissection, a paradigm established by certain genetic and syndromic aortopathies [11–13]. A role for dysfunctional SMC in BAV aortopathy is less clear, although SMC abnormalities have been identified. This includes SMC apoptosis [14–16] which, if greater than SMC replication, could lead to SMC loss. Defects in SMC differentiation and maturation have also been reported in BAV aortopathy [17–21]. SMCs that are not highly differentiated can promote ECM degradation through elaboration of matrix metalloproteinases (MMPs), which have been identified in the BAV aorta [17,22]. However, SMC apoptosis by itself is unlikely to contribute to the ECM breakdown of aortopathy and less differentiated SMCs can be fundamental to vascular repair. What determines a destructive versus reparative SMC in the ascending aorta remains unknown.

Another cellular fate that is known to compromise tissue health is senescence. Cellular senescence is a state of essentially permanent cell cycle arrest but with ongoing metabolic activity. Cells become senescent in response to certain triggers, including unrepaired DNA damage and burdens of oxidative stress [23]. Of particular importance to tissues that accrue senescent cells is a transcriptionally-driven shift in the secretome of these cells, referred to as the senescence-associated secretory phenotype (SASP) [24,25]. The components of SASP can vary depending on cell type and context [26], but altered MMP production is a common feature [27]. Data on the extent and consequences of SMC senescence in the vasculature is limited, particularly in humans. However the propensity for human vascular SMCs to become senescent in culture is well recognized [28], and senescent SMCs have been identified in advanced human atherosclerotic lesions [29]. Interestingly, SMCs cultured from BAV ascending aortas have been reported to have shortened telomeres and increased transcript abundance of cell-cycle inhibitors [30,31]. Whether overtly senescent SMCs exist within aneurysmal or

at-risk ascending aortas is unclear. Moreover, whether a senescent cell in this context has consequences is unknown.

Herein, we report that senescent SMCs accumulate in aneurysmal ascending aortas associated with bicuspid and tricuspid aortic valves. Moreover, we identified a particular predisposition to SMC senescence in BAV aortopathy, indicated by the presence of senescent SMCs in non-aneurysmal BAV aortas, enrichment of cellular senescence at the aortic convexity, and multivariable analysis of potential aneurysm risk factors. We further show that senescent aortic SMCs have a pronounced collagenolytic SASP, a destructive profile that is controlled by p38 MAPK. The findings identify a cellular aging cascade in human BAV disease and a “seno-destructive” SMC phenotype that may underlie the aortic wall degeneration.

**2. Materials and methods***2.1. Procurement of ascending aorta tissue*

The study complies with the Declaration of Helsinki and was carried out with approval of the Western University Research Ethics Board. Ascending aortic tissue was harvested from subjects with either bicuspid or tricuspid aortic valves at the time of thoracic aorta replacement surgery. Patients with genetic or syndromic aortopathy, including connective tissue disorders, were excluded. Ascending aortic tissue was also harvested during elective coronary artery bypass surgery or at the time of heart transplantation. Informed consent was obtained from all subjects, with the exception of heart transplant donors and one heart transplant recipient. In the latter instances, normally discarded tissue with no patient identifiers was studied. These aortic samples were histologically non-diseased. Aortic tissue was categorized into four groups: TAV-non-aneurysm (TAV-NA,  $n = 15$ ), BAV-non-aneurysm (BAV-NA,  $n = 10$ ), TAV-aneurysm (TAV-A,  $n = 14$ ), BAV-aneurysm (BAV-A,  $n = 28$ ). Aortic aneurysm was defined as having a body-surface area (BSA)-normalized diameter of  $\geq 2.1$  cm/m<sup>2</sup>, based on published data [32–35]. This threshold was refined for extremes of body size to account for overcorrection [35]. For a BSA  $\leq 1.5$  m<sup>2</sup>, aortas were deemed aneurysmal if the BSA-normalized diameter was  $\geq 2.1$  cm/m<sup>2</sup> and the absolute diameter was  $\geq 4.0$  cm. For BSA  $\geq 2.5$  m<sup>2</sup> the threshold was an absolute diameter  $\geq 4.5$  cm. For the 12 BAV-non-aneurysm aortas the indication for aortic replacement was driven by the co-existing aortic valve/root disease. In 22 instances, a full circumferential ring of aortic tissue was harvested, with the convexity denoted with an adventitial suture. Aortic valve morphology was determined from the pre-operative echocardiogram and confirmed intraoperatively.

Tissues were divided so that a  $\sim 4.0 \times 0.3$  cm fragment was used for SMC culture, a  $\sim 1.5 \times 0.5$  cm fragment was assessed immediately for SA- $\beta$ Gal activity, and the remaining and generally largest fragment was fixed in 10% neutral buffered-formalin. The diameter of the ascending aorta at the level of the right pulmonary artery was measured from the double-oblique short axis plane of 3D reconstructed, contrast-enhanced multi-detector helical CT images. All procedures involving human bio-specimens adhered to the BRISQ guidelines.

*2.2. Senescence-associated  $\beta$ -galactosidase activity in aortic tissue*

Immediately upon harvesting, an aortic tissue fragment was incubated in senescence-associated  $\beta$ -galactosidase staining solution (1 mg/ml 5-bromo-4-chloro-3-indolyl  $\beta$ -D-Galactosidase (X-gal), 40 mM citric acid/sodium phosphate (pH 6.0), 5 mM potassium ferrocyanide, 5 mM potassium ferricyanide, 150 mM sodium chloride, 2 mM magnesium chloride) for 12 h at 37 °C. Tissues were washed twice with PBS, fixed with 10% formalin for 4 h, and cryoprotected in 30% sucrose overnight at 4 °C and embedded in OCT (Optical Cutting Temperature, Tissue-Tek®). Cryosections were then immunostained for the leukocyte cell surface marker, CD45 (see below), and non-leukocyte,

SA- $\beta$ Gal-positive cells in the section were counted and expressed as a percentage of all SMCs.

### 2.3. Immunohistochemistry

OCT-embedded sections of X-gal-incubated tissues and formalin-fixed, paraffin-embedded aortic tissue sections were immunostained using mouse antibodies against human smooth muscle  $\alpha$ -actin (M-0851, 1:300, Agilent Technologies, Santa Clara, CA, USA, RRID: [AB\\_2223500](#)) and p16<sup>Ink4a</sup> (sc-1661, 1:100; Santa Cruz Biotechnology, Mississauga, ON, Canada, RRID: [AB\\_628067](#)) and rabbit anti-human CD45 (ab10558, 1:500; Abcam, Toronto, ON, Canada, RRID: [AB\\_442810](#)) or p21 (SC-756, 1:200, Santa Cruz Biotechnology, RRID: [AB\\_2229243](#)). Bound primary antibodies were detected using horseradish peroxidase-labeled sheep anti-mouse IgG antibody (NXA931, 1:200, Sigma-Aldrich, Oakville, ON, Canada, RRID: [AB\\_772209](#)) or horseradish peroxidase-labeled donkey anti-rabbit IgG (NA934V, 1:200, GE Healthcare Life Sciences, Mississauga, ON, Canada, RRID: [AB\\_772206](#)). Antibodies were visualized with ABC reagent and diaminobenzidine (DAB, Vector Laboratories, Burlington, ON, Canada). Sections were counterstained with Harris' hematoxylin. The proportion of immune-positive cells were quantified from eight to ten evenly distributed regions (x20 objective) from the middle third of the aortic media. Sections were also double-immunostained for SM- $\alpha$ -actin (ab5694, 1:300, Abcam, RRID: [AB\\_2223021](#)) and p16<sup>Ink4a</sup> (F-12, Santa Cruz Biotechnology), with bound primary antibodies detected with Alexa Fluor 488-conjugated goat anti-rabbit (1:500, RRID: [AB\\_143165](#)) and Alexa Fluor 546-conjugated goat anti-mouse secondary antibodies (1:500, ThermoFisher Scientific, Burlington, ON, Canada, RRID: [AB\\_144695](#)). As well, sections were double-labeled with SM- $\alpha$ -actin (M-0851, 1:300, Agilent Technologies) and p21 (sc-756, 1:200, Santa Cruz Biotechnology) and visualized with Alexa Fluor 488-conjugated goat anti-mouse (1:500, ThermoFisher Scientific, RRID: [AB\\_138404](#)) and DyLight 549-conjugated goat anti-rabbit secondary antibodies (1:500, Vector Laboratories, RRID: [AB\\_2336407](#)). Sections were imaged with a Leica TCS SP8 confocal laser scanning microscope, 63 $\times$  oil-immersion objective and Diode 405, OPAL 488, OPAL 552 and Diode 638 lasers to generate 0.9- $\mu$ m-thick z-slices at a pixel resolution of 59 nm. Z-axis maximal intensity projections were generated using LAS X software based on image stacks with a z-step size of 0.3  $\mu$ m and spanning a total of 3  $\mu$ m.

To assess for DNA damage, sections were double-immunostained using rabbit anti-human  $\gamma$ H2AX (9718, 1:50, Cell Signaling, Danvers, MA, USA, RRID: [AB\\_2118009](#)) and the proliferation marker, mouse anti-human Ki67 (M-7240, 1:50, Agilent Technologies, RRID: [AB\\_2142367](#)). Bound antibodies were detected using DyLight<sup>®</sup> 488-conjugated goat anti-rabbit (1:100, Vector Laboratories, RRID: [AB\\_2336402](#)) and Alexa Fluor 546-conjugated goat anti-mouse (1:100, ThermoFisher Scientific) secondary antibodies, respectively. Sections were mounted with DAPI-supplemented VECTASHIELD Mounting Media (Vector Laboratories). Tissues were imaged using epifluorescence microscopy (Olympus BX51, UPlan S Apo objectives, cooled Retiga EXi Mono Fast 1394 camera (Q-imaging Inc.) or Leica SP8 and 8–10 images/aorta captured using Northern Eclipse image analysis software. Cells with at least five, discrete  $\gamma$ H2AX nuclear foci were deemed positive for unrepaired DNA damage and the proportion of  $\gamma$ H2AX-positive/Ki67-negative nuclei was determined from a minimum of 500 SMCs per tissue. Maximal intensity projections were generated from serial 0.3  $\mu$ m-stacks spanning 5  $\mu$ m.

In situ p38 MAPK activity was assessed by immunostaining for rabbit anti-human phosphorylated p38 MAPK (T180/Y182; 8690, 1:100, Cell Signaling, RRID: [AB\\_10999090](#)), visualized with goat anti-rabbit DyLight<sup>®</sup> 594-conjugated secondary antibody (1:500, Vector Laboratories, RRID: [AB\\_2336413](#)). The association of MMP1 and p16 expression was assessed by double-immunolabelling, using mouse anti-human p16 (F-12, 1:100) and rabbit anti-human MMP1 (ab52631, 1:50, Abcam, RRID: [AB\\_2144301](#)), differentially visualized with secondary

antibodies against donkey anti-mouse conjugated to Alexa Fluor 488 (1:500, RRID: [AB\\_141607](#)) and donkey anti-rabbit conjugated to Alexa Fluor 594 (1:1000, ThermoFisher Scientific, RRID: [AB\\_141637](#)), respectively. Fluorescent intensity of MMP1 signal within the aortic media was quantified, with identical exposure times, as the mean intensity from eight to twelve evenly distributed medial zones (x20 objective) using ImageJ. To quantify the MMP1 signal intensity associated with individual SMCs, a rectangular field of view measuring 10  $\times$  90  $\mu$ m was superimposed over each cell, centered over the nucleus. These dimensions corresponded to the average aortic inter-lamellar distance (10.4  $\pm$  0.6  $\mu$ m,  $n$  = 90) and the average of seven nuclear lengths (89.7  $\pm$  1.1  $\mu$ m,  $n$  = 90).

### 2.4. Aortic SMC isolation and culture

SMCs were cultured by outgrowth from explanted fragments of aortic media. Endothelial cells were removed by scraping the luminal surface with a scalpel blade and the adventitia and outermost media peeled away with forceps and surgical scissors. The resulting fragment was cut into  $\sim$ 1  $\times$  1 mm pieces, placed on culture dishes pre-coated with 0.4% gelatin, and incubated in M199 media supplemented with 10% fetal bovine serum (FBS, Invitrogen, Burlington, Canada). Cell population doubling rate was determined as previously reported [36].

SA- $\beta$ Gal activity was assessed in SMCs fixed in 2% formaldehyde/0.2% glutaraldehyde in PBS for 3 min and incubated with X-gal staining solution, as above. Nuclei were stained with Hoechst 33258 (2.5  $\mu$ g/ml) and the proportion of SA- $\beta$ Gal-positive cells was quantified from a total of  $\sim$ 500 cells per patient sample or experimental condition.

p38 activity was inhibited by incubating cultures with SB203580 (Cell Signaling) at 10  $\mu$ M daily. p38 expression was knocked down using siRNA against p38 MAPK (50 nM, Ambion), delivered using lipofectamine-assisted transfection (Lipofectamine<sup>®</sup> RNAiMAX, Thermo Fisher). Negative Control siRNA #1 (50 nM, Applied Biosystems) was similarly delivered as control.

### 2.5. Real-time quantitative RT PCR

Total RNA was isolated from BAV and control SMCs with the Qiagen RNeasy kit (Qiagen, Mississauga, ON, Canada). RNA concentration was determined using a NanoDrop ND-1000 spectrophotometer (Thermo Scientific, Mississauga, ON, Canada). Complementary DNA was synthesized with Multiscribe Reverse Transcriptase (Applied Biosystems, Streetsville, ON, Canada) and amplified through real-time RT PCR (ABI 7900HT Fast Real-Time PCR apparatus and Sequence Detection System software). Primers for senescence marker genes and secreted gene products were custom-designed (OriGene) and synthesized (Sigma) (Supplemental Table S1). Quantification of relative mRNA abundance based on critical threshold (CT) was assessed using 18 s mRNA as the internal control.

### 2.6. Collagen fibril assessment by circular polarization microscopy

Paraffin-embedded sections were stained with picosirius red (Polysciences, Warrington, PA, USA) and collagen fibrils imaged by circular polarization microscopy, using an Olympus BX51 microscope equipped with Olympus BX series circular polarizer/interference filters, a liquid crystal compensator and CCD camera, and processing software (Abrio LC-PolScope, Cambridge Research & Instrumentation, Woburn, MA, USA). To assess for the integrity of collagen fibrils specifically around senescent SMCs, we developed a strategy to immunostain sections for p16<sup>Ink4a</sup> and also stain for picosirius red. Briefly, p16<sup>Ink4a</sup> immunoreactivity was developed using a black chromogen (Deep Space Black chromogen kit, Biocare Medical, Pacheco, CA, USA) and nuclei were lightly counterstained using celestine blue (Sigma-Aldrich)-alum hematoxylin (Leica Biosystems, Concord, ON, Canada), followed by picosirius red staining. The resulting p16<sup>Ink4a</sup> and nuclear signals

were thus both resistant to acidic condition of picosirius red staining. Fields containing p16<sup>Ink4a</sup>-positive SMCs were captured with bright-field microscopy and correspondingly recaptured under circular polarized light microscopy. To assess for collagen integrity associated with each cell, 10  $\mu\text{m}$   $\times$  90  $\mu\text{m}$  rectangular fields of view described above were superimposed over each cell. The mean light retardation (nm) by collagen fibrils associated with p16<sup>Ink4a</sup>-expressing SMCs was determined and expressed relative to that of non-senescent cells in the same section.

### 2.7. Statistics

The target sample size was based on a preliminary study of p16<sup>Ink4a</sup> immunoreactivity in 5 aortas from each group which yielded an estimated effect size (expressed as the ratio of between-group to common within-group standard deviation (SD)) of 0.83. This translated to a target sample size of 8 subjects per group, with a power of 95% and  $\alpha$  of 0.05. Descriptive subject data are presented as mean  $\pm$  standard deviation (SD). Aortic tissue and cell culture data obtained for group comparisons are presented as mean  $\pm$  standard error of the mean (SEM). All data distributions were tested for normality using the D'Agostino and Pearson omnibus normality test. Comparisons among normal distributions were made by *t*-test and among non-normal distributions by Mann-Whitney *U* test. Non-normal distributions existed for p21-, SA- $\beta$ Gal- and phospho-p38 MAPK-positive SMCs in control aortas, pericellular collagen birefringence in control aortas, and p16<sup>Ink4a</sup> and p21 mRNA abundance in cultured SMCs. Comparisons between more than two groups were undertaken using analysis of variance with Bonferroni's post-hoc test (normal distributions) or Kruskal-Wallis test with Dunn's post-hoc test (non-normal distributions). Transcript expression differences between BAV and control SMCs were assessed with *P* values adjusted for multiple testing using the Benjamini-Hochberg procedure at false discovery rate of 0.05. To determine if bicuspid aortic valve was an independent risk factor for SMC senescence, we performed multiple linear regression with adjustment for ascending aortic diameter and age, for each of the measured senescence markers. Linear regression analyses were used to assess relationships between continuous variables. Statistical analyses were performed using Prism 7 (Graphpad Software) and SPSS 19 (IBM Corp., Armonk, New York).

## 3. Results

### 3.1. A proportion of medial SMCs in BAV and TAV adult aortas undergo premature senescence

Ascending aortic tissue from 68 subjects was harvested. Aortas were categorized into four groups based on valve cuspidity and aortic dimensions: TAV-non-aneurysm (TAV-NA, *n* = 15), BAV-non-aneurysm (BAV-NA *n* = 10), TAV-aneurysm (TAV-A, *n* = 14), BAV-aneurysm (BAV-A, *n* = 29). Clinical information for all subjects is presented in Table 1 and Supplemental Tables S2–S5. To seek evidence for SMC senescence, tissues were immunostained for p16<sup>Ink4a</sup> and p21, cyclin-dependent kinase inhibitors (CDKI) that define the two core senescence induction pathways [23,25]. Interestingly, this revealed scattered immuno-positive SMCs in the media of TAV-NA aortas - 7.5  $\pm$  1.1% for p16<sup>Ink4a</sup> and 2.2  $\pm$  0.6% for p21 (Fig. 1a,b). However, in BAV-NA aortas, the proportion of p16<sup>Ink4a</sup>-positive SMCs was 3.2-fold greater (*P* = .0009), and the proportion of p21-positive SMCs 10.9-fold greater (*P* < .0001) (Fig. 1a-c). Aneurysmal aortas, either TAV-A or BAV-A, also had abundant p16<sup>Ink4a</sup>-expressing and p21-expressing SMCs, significantly more than in TAV-NA aortas (*p* < .01 or less) but on average not different than in BAV-NA aortas (Fig. 1a-c). Double-labeling for p16<sup>Ink4a</sup> and SM- $\alpha$ -actin and for p21 and SM- $\alpha$ -actin supported the identity of the CDKI-positive cells as SMCs (Fig. 1d).

We also assayed fresh aortic tissue for SA- $\beta$ Gal activity, a senescence biomarker that reflects lysosomal expansion. There was no SA- $\beta$ Gal

**Table 1**  
Clinical characteristics of study subjects.

Characteristics	TAV-NA	BAV-NA	TAV-A	BAV-A
Number (female)	15 (5)	10 (2)	14 (6)	29 (5)
Age (y)	66 $\pm$ 23	47 $\pm$ 13 <sup>b</sup>	69 $\pm$ 13	59 $\pm$ 15
Hypertension, n (%)	4 (40) <sup>a</sup>	2 (20)	10 (71)	18 (62)
Diabetes, n (%)	5 (50) <sup>a</sup>	2 (20)	2 (14)	2 (7)
Smoking, n (%)	4 (40) <sup>a</sup>	6 (60)	4 (29)	10 (35)
Aortic stenosis n (%)	0 (0) <sup>a</sup>	5 (50)	0 (0)	16 (55)
Aortic regurgitation	0 (0) <sup>a</sup>	5 (50)	4 (29)	17 (59)
Maximum Ascending Aorta Diameter (cm)	3.2 $\pm$ 0.4	3.7 $\pm$ 0.4	5.3 $\pm$ 0.8 <sup>c</sup>	5.1 $\pm$ 0.5 <sup>c</sup>
Maximum Ascending Aorta Diameter (cm/m <sup>2</sup> )	1.9 $\pm$ 0.3	1.9 $\pm$ 0.3	2.7 $\pm$ 0.4 <sup>c</sup>	2.6 $\pm$ 0.3 <sup>c</sup>

<sup>a</sup> *n* = 10.

<sup>b</sup> *P* = .049 vs TAV-NA.

<sup>c</sup> *P* < .0001 vs TAV-NA and BAV-NA.

activity detected among CD45-negative medial cells in 10 of 13 TAV-NA aortas, and fewer than 0.1% SA- $\beta$ Gal-positive cells in the remaining three aortas. However, there were SMCs with SA- $\beta$ Gal activity in all BAV-NA aortas (2.8  $\pm$  0.8% of CD45-negative medial cells, *P* = .017) (Fig. 1e,f). SA- $\beta$ Gal activity was also prevalent in the media of TAV-A aortas (5.2  $\pm$  0.8%, *P* < .0001) and BAV-A aortas (5.8  $\pm$  1.2%, *P* < .0001) (Fig. 1e,f). Double-staining for SA- $\beta$ Gal activity and p16<sup>Ink4a</sup> revealed that almost all SA- $\beta$ Gal-positive SMCs also expressed p16<sup>Ink4a</sup>. In contrast, most p16<sup>Ink4a</sup>-expressing SMCs did not have demonstrable SA- $\beta$ Gal activity (Fig. 1e). Double-labeling for SA- $\beta$ Gal activity and SM  $\alpha$ -actin confirmed the identity of SA- $\beta$ Gal-positive cells as SMCs (Fig. 1e).

These data reveal that senescent SMCs can be found in the media of adult ascending thoracic aortic, and are particularly prevalent in aneurysms and in BAV aortas that have not yet progressed to an aneurysmal state. The multi-marker characterization and lower prevalence of SA- $\beta$ Gal-activity also suggests that aortic SMCs can exist within a spectrum of senescence [37], with CDKI/SA- $\beta$ Gal-double-positive SMCs likely having a deeper level of senescence than the more prevalent CDKI-single-positive SMCs.

### 3.2. SMCs in BAV aortas have an increased predisposition to senescence

The observation that non-aneurysmal BAV aortas contained SA- $\beta$ Gal-positive SMCs, and significantly more CDKI-expressing SMCs than non-aneurysmal TAV aortas, suggested a predisposition to SMC senescence in BAV disease. At the same time, SMC senescence was not specific to BAV aortopathy. Therefore, to further assess if BAV disease, per se, increased the likelihood of SMC senescence, we undertook multiple linear regression modeling. Specifically, for all 68 patients, the relationships between the prevalence of cellular senescence biomarkers and patient age, aortic diameter, and valve cuspidity were modeled. Interestingly, this revealed that in this population patient age was not found to be an independent predictor of SMC senescence. However, aortic diameter independently associated with the abundance of p16<sup>Ink4a</sup>- and SA- $\beta$ Gal-positive SMCs (Table 2, Fig. 2a), and BAV disease independently associated with the abundance of each of the three markers of SMC senescence (Table 2). Because aortic stenosis has been associated with short leukocyte telomeres [38], we also examined whether aortic valve stenosis or regurgitation associated with aortic wall SMC senescence. However, the prevalence of aortic wall SMC senescence among patients with either aortic stenosis or aortic regurgitation ( $\geq$  moderate) did not differ from that in those without aortic valve dysfunction (*p* > .10 for all three senescence biomarkers), suggesting that differences in stenosis or regurgitation did not account for the heightened cellular senescence in BAV aortas vs. TAV aortas. Together with the biomarker staining data, these findings suggest a propensity to SMC senescence in BAV disease, in addition to that imposed by aortic dilation itself.

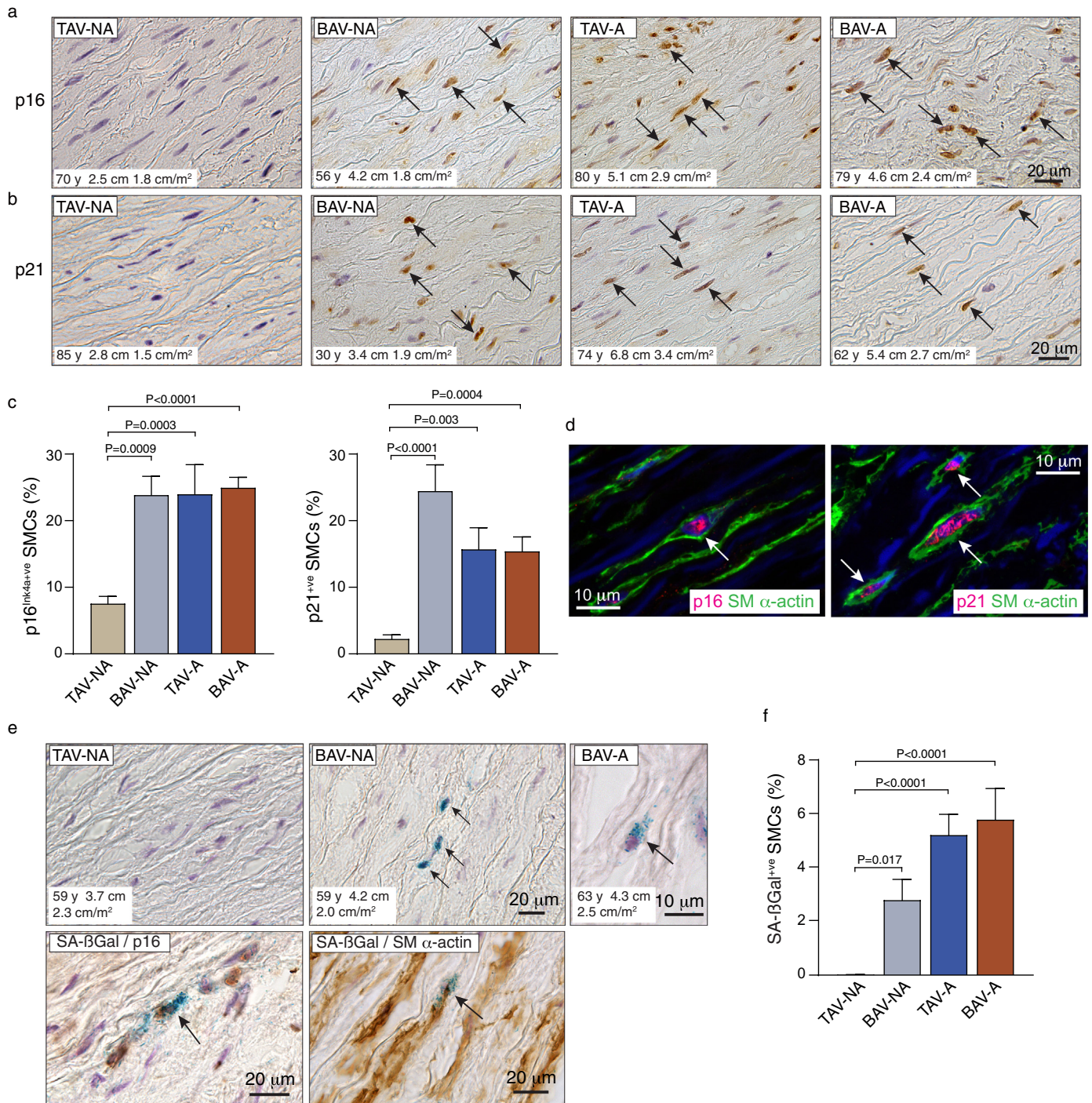


**Fig. 1.** Senescent medial SMCs in the ascending aorta of patients with BAV and TAV. (a) Bright-field microscope images of sections of aortas immunostained for p16<sup>Ink4a</sup>. Nuclei were counterstained with hematoxylin and brown (DAB) signal within the nuclei (arrows) indicate immuno-positive medial cells (BAV, bicuspid aortic valve; TAV, tricuspid aortic valve; NA-non-aneurysmal; A, aneurysmal). (b) Sections of ascending aortas immunostained for p21. (c) Graphs depicting quantitative data for p16<sup>Ink4a</sup> and p21 expression. (d) Confocal images from a BAV aorta triple-labeled for SM  $\alpha$ -actin (green), p16<sup>Ink4a</sup> (red) or p21 (red), and with DAPI (blue), confirming SMCs as expressing the senescence markers (arrows). (e) *Top*: Bright-field images of sections of TAV and BAV aortas assessed for senescence-associated  $\beta$ -galactosidase (SA- $\beta$ Gal) activity, immunostained for CD45, and counterstained with hematoxylin. Senescent medial SMCs are evident by the blue perinuclear SA- $\beta$ Gal signals and lack of brown CD45 signal (arrows). *Bottom*: Image of BAV aorta section double-labeled for SA- $\beta$ Gal activity and p16<sup>Ink4a</sup> (brown). Dual-labeled image on right depicts SA- $\beta$ Gal activity in a SM  $\alpha$ -actin-expressing (brown) medial cell (arrow). (f) Graph showing the proportion of SA- $\beta$ Gal-positive SMCs (TAV-NA  $n = 13$ , BAV-NA  $n = 10$ , TAV-A  $n = 14$ , BAV-A  $n = 19$ ).

### 3.3. SMC senescence is enriched at the convexity of BAV-associated ascending aortas

Fusion of the right and left coronary aortic cusps directs flow toward the convex region of the ascending aorta, a zone that has been reported

to be preferentially damaged [2]. Among all BAV patients, 68% had fusion of the right and left coronary cusps with a single raphe (Sievers classification Type 1; L-R). Among 15 individuals in whom a full circumference aortic tissue was retrieved ( $n = 3$  BAV-NA,  $n = 12$  BAV-A), the proportion of p16<sup>Ink4a</sup>-positive SMCs was 1.4-fold higher at the

**Table 2**

Association of senescence markers with cuspidity, patient age, and aortic diameter.

Senescence marker	Independent variable	Beta	SE	P
SA-βGal	BAV	2.302	1.001	0.026*
	Age	0.032	0.030	0.289
	Aortic diameter	0.441	0.101	<0.0001*
p16 <sup>Ink4a</sup>	BAV	8.259	2.981	0.008*
	Age	0.065	0.089	0.474
	Aortic diameter	0.914	0.302	0.003*
P21	BAV	7.040	3.379	0.042*
	Age	-0.043	0.100	0.630
	Aortic diameter	0.344	0.342	0.318

SE, standard error

\* P < .05.

convexity than the concavity (P = .039) and the proportion of p21-positive SMCs was 1.3-fold higher (P = .002; Fig. 2b). We did not detect spatial differences in SA-βGal activity among BAV aortas, recognizing however the comparatively low prevalence of SA-βGal-positive SMCs. No regional differences in the proportion of CDKI-positive SMCs was evident in those BAV aortas with other than R-L coronary cusp fusion (P = .511, P = .212). Likewise, regionalization of senescence was not evident in TAV aneurysms (P = .250, P = .563).

**3.4. SMCs in the BAV-associated aorta accumulate unrepaired double-strand DNA breaks**

Unrepaired double-strand DNA breaks are a driver of cellular senescence [23]. To determine if damaged DNA could be detected in the ascending aorta, we double-immunostained for Ki67 and the double-strand break signal, phosphorylated histone γ-H2AX. Interestingly, this revealed DNA damage foci in non-proliferating SMCs within control TAV-NA aortic tissue, with an average of 4.2 ± 1.0% of SMCs having unrepaired DNA lesions (Fig. 3). However, the prevalence of DNA lesions in the each of three other groups was substantially higher - 3.7-fold higher for BAV-NA aortas (P = .0002), 2.9-fold higher for TAV-A aortas (P = .008), and 3.4-fold higher for BAV-A aortas (P < .0001, Fig. 3a,b). The abundance of γH2AX-positive SMCs correlated with SA-βGal activity (r = 0.37, P = .005), p16<sup>Ink4a</sup> (r = 0.49, P < .0001) and p21 (r = 0.61, P < .0001) (Fig. 3c).

**3.5. Senescent aortic SMCs from patients with BAV have a collagen-degrading secretory profile**

Senescent cells have a distinct secretory phenotype (SASP) which can extend the impact of senescence beyond the cell itself [24]. SASP components differ among different cell types and many are upregulated transcriptionally [26]. To investigate the potential for senescent

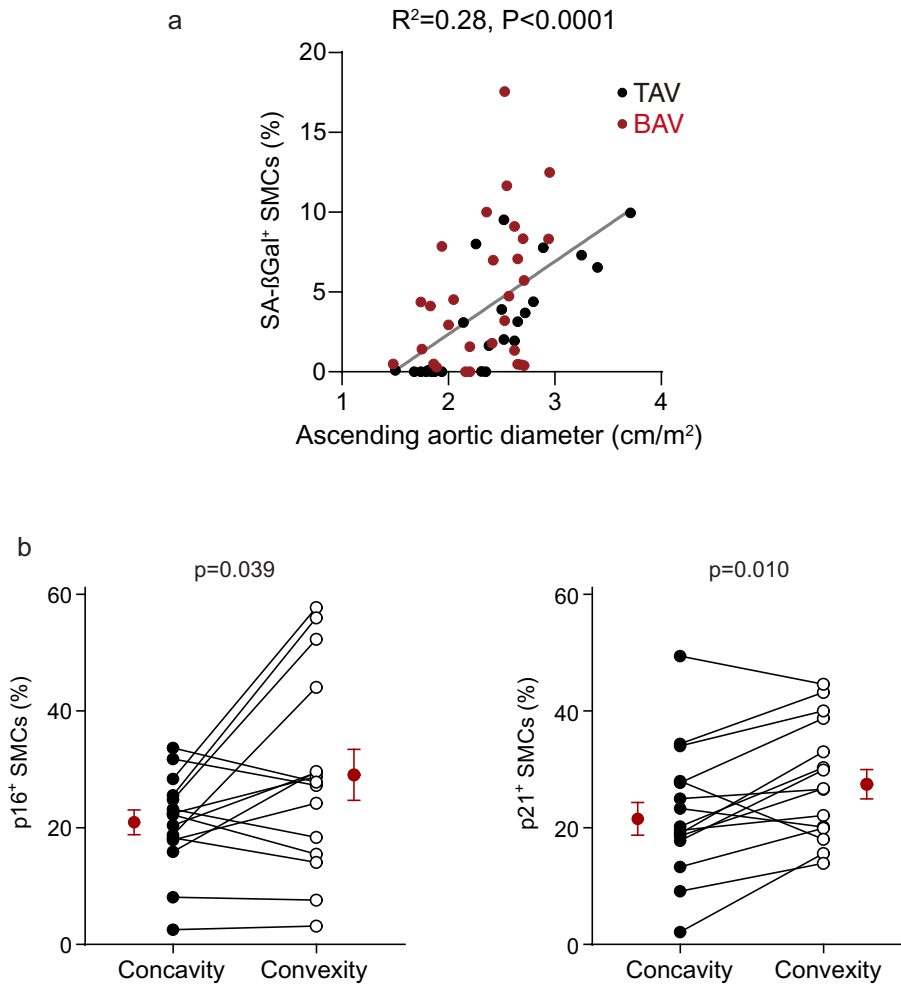


**Fig. 2.** Association of SMC senescence with ascending aortic diameter and convexity in BAV aortas. (a) Scatterplot depicting the relationship between SA-βGal-positive SMCs and ascending aortic diameter. (b) Graphs comparing p16<sup>Ink4a</sup> and p21 expression in SMCs at the aortic concavity vs. convexity in full-circumference BAV aortic sections (n = 15). Mean data are in red.

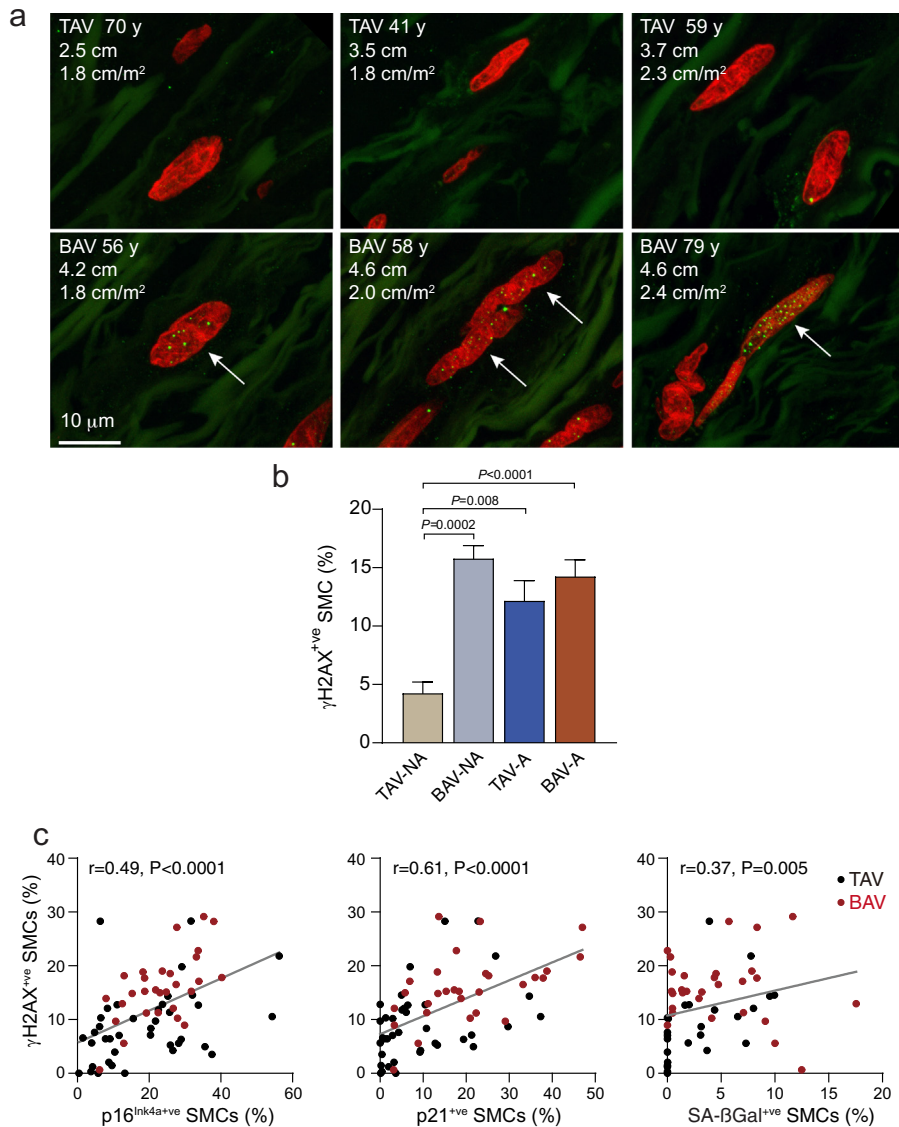


**Fig. 3.** Accumulation of unrepaired double-strand DNA breaks in medial SMCs in BAV aortas. (a) Confocal images of aortic cross-sections of TAV-NA (top), BAV-NA and BAV-A subjects (bottom) labeled for  $\gamma$ H2AX foci (green). Nuclei were counterstained with propidium iodide (red). (b) Graphs depicting the proportion of medial SMCs with nuclear  $\gamma$ H2AX foci in TAV-NA ( $n = 15$ ), BAV-NA ( $n = 12$ ), TAV-A ( $n = 14$ ) and BAV-A ( $n = 28$ ) aortas. (c) Plots depicting correlations between abundance of  $\gamma$ H2AX-positive medial SMCs and that of p16<sup>Ink4a</sup>-positive (left), p21<sup>+ve</sup>-positive (middle) or SA- $\beta$ Gal<sup>+ve</sup>-positive (right) SMCs.

BAV-associated SMCs to impact their environment, we evaluated a panel of transcripts encoding secreted gene products in SMCs harvested from 10 BAV aortas (5 BAV-NA and 5 BAV-A). SMCs were subjected to an additional 5 weeks of culture-induced aging which yielded  $41 \pm 5\%$  SA- $\beta$ Gal-positive SMCs. This did not differ between BAV-NA and BAV-A SMCs. Given this, and the similar senescence profiles in situ, BAV-NA SMCs and BAV A SMCs were considered as a single population. Transcript abundance was compared to that of SMCs from four TAV-NA aortas subjected to identical culture conditions. The latter SMCs displayed more robust growth (50% shorter doubling time,  $P = .021$ ) and 48% fewer SA- $\beta$ Gal-positive cells ( $P = .019$ ).

Fig. 4 depicts hierarchically clustered mRNA expression data for 13 MMPs, four TIMPs, nine collagen  $\alpha$ -chains, and six inflammatory cytokines, with multiple-test corrected  $P$  values for all differences. Interestingly, all three interstitial collagenases were upregulated in aged BAV SMCs - MMP1 (10.2-fold), MMP8 (2.2-fold), and MMP13 (3.4-fold) - with a trend to upregulated MMP2. In contrast, the stromelysins MMP3, MMP10, and MMP11 were down-regulated, as was the elastase, MMP12. Transcript abundance of membrane-type MMPs (MMP14, 15,

16) was not different between SMC types. However, all four TIMPs (TIMPs1–4) were significantly down-regulated, with TIMP1 decreased by 94% in BAV aortic SMCs. As well, expression of COL1A1, COL1A2, and COL3A1, which encode the main interstitial collagen  $\alpha$ -chains within human aorta, were all significantly decreased in aged BAV aortic SMCs. COL12A1, which encodes the  $\alpha$ -chain for the type I collagen-interacting type XII collagen was also downregulated. TGF- $\beta$ 1 abundance was increased in the senescence-enriched BAV aortic SMCs however there were no increases in TNF- $\alpha$ , IL-1 $\beta$ , IL-6 or MIP1- $\alpha$  expression, and MCP-1 expression was significantly lower.

Collectively, these data suggest that senescent BAV aorta SMCs are programmed for depleting collagen fibrils, via a collagenolysis- and collagen gene suppression-related SASP.

### 3.6. BAV-associated aortas contain senescent, MMP1-expressing SMCs

To determine if the collagen-degrading attribute of aged BAV aorta-derived SMCs existed in the aortic wall, we immunostained human aortic tissue for MMP1, the canonical fibrillar collagen-degrading enzyme

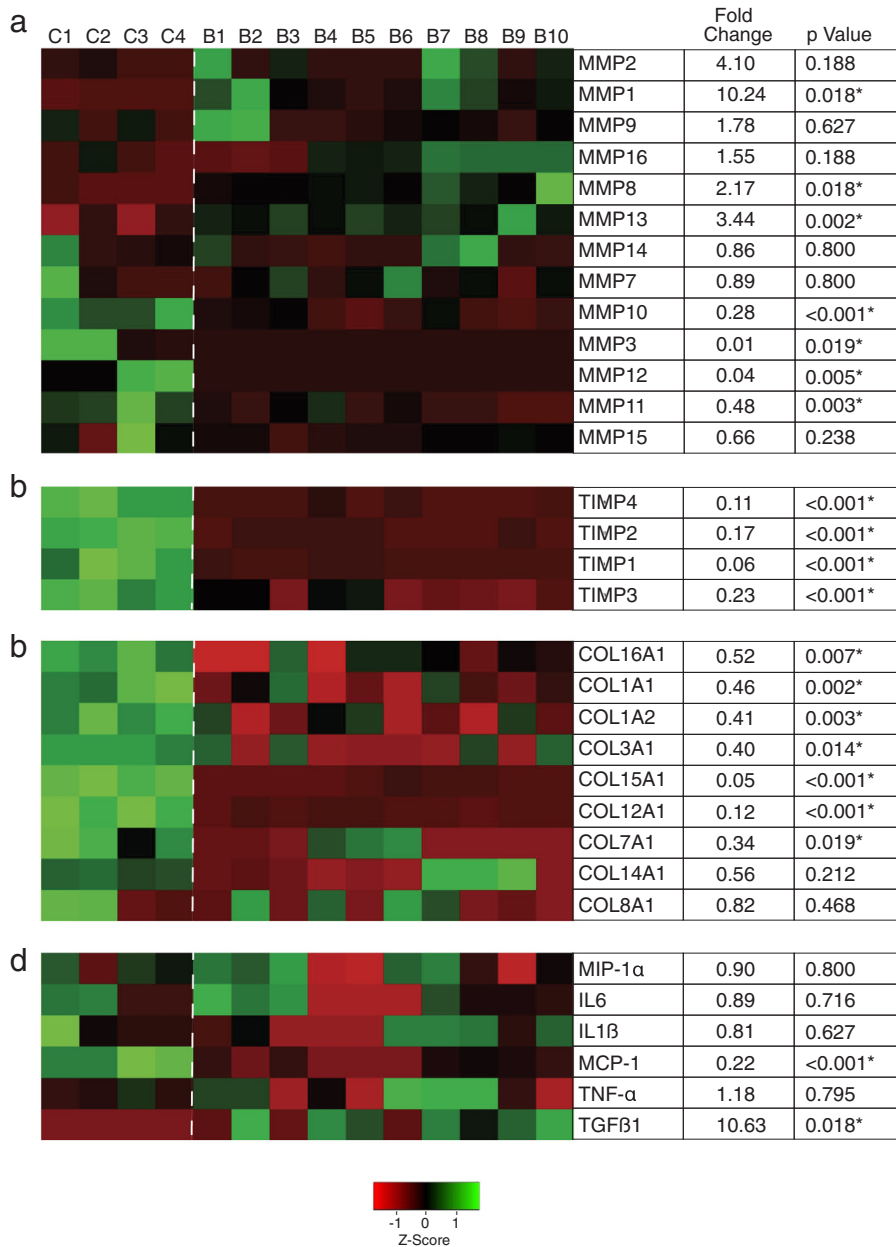


**Fig. 4.** Secretory profile of ascending aortic SMCs from patients with and without BAV. Abundance of transcripts encoding secreted factors in SMCs cultured from control (C1–C4) and BAV subjects (B1–B10), assessed using reverse transcription-quantitative PCR. Heat maps were generated from unsupervised hierarchical clustering. Green and red shades represent high and low abundance, respectively. \*multiple test-adjusted  $P < .05$ .

in the vasculature. Control (TAV-NA) aortic tissues were found to have weak MMP1 signal that was primarily cell-associated (Fig. 5a–c). In contrast, in either BAV-NA or BAV-A aortas, SMCs with pronounced MMP1 expression were evident. Particularly strong signal was evident at the cell periphery, suggesting MMP1 localized at the cell surface (Fig. 5d–h).

To further assess the linkage between MMP1 and senescence, tissues were double-labeled for MMP1 and p16<sup>Ink4a</sup>. This revealed intense MMP1 signal associated with p16<sup>Ink4a</sup>-positive SMCs (Fig. 5f–h). Heightened MMP1 expression by senescent SMCs was particularly appreciable in regions where p16<sup>Ink4a</sup>-positive SMCs were adjacent to p16<sup>Ink4a</sup>-negative SMCs (Fig. 5h). Quantitation revealed a 1.7-fold greater MMP1 signal in the media of BAV aortas than in control, TAV-A aortas ( $P = .0009$ , Fig. 5i). Furthermore, within a given BAV aorta, the intensity of cell-associated MMP1 signal in p16<sup>Ink4a</sup>-expressing SMCs was 2.5-fold greater than that in p16<sup>Ink4a</sup>-negative SMCs ( $P < .0001$ , Fig. 5j).

### 3.7. Senescent SMCs in BAV aortas are surrounded by disrupted collagen fibrils

To determine if the senescent SMCs were linked to aortic degeneration, we examined the state of collagen fibrils using circular polarization microscopy. This revealed that, in control TAV-NA aortas, fibrillar collagen existed as concentric bands of birefringent fibrils on either side of each elastic lamella (Fig. 6a). In BAV-NA and BAV-A aortas, these bands could be discontinuous, thinner, and less birefringent. This disrupted collagen pattern was particularly evident surrounding p16<sup>Ink4a</sup>-positive SMCs (Fig. 6a,b). Overall, among 10 BAV aortas (2 BAV-NA, 8 BAV-A) there was a 43% reduction in total medial collagen content and a 35% reduction in collagen fibril retardation compared to TAV-A aortas (Fig. 6c,d).

Using a co-immuno-labeling and circular polarized light imaging strategy, we also found that, within BAV aortas and on an individual

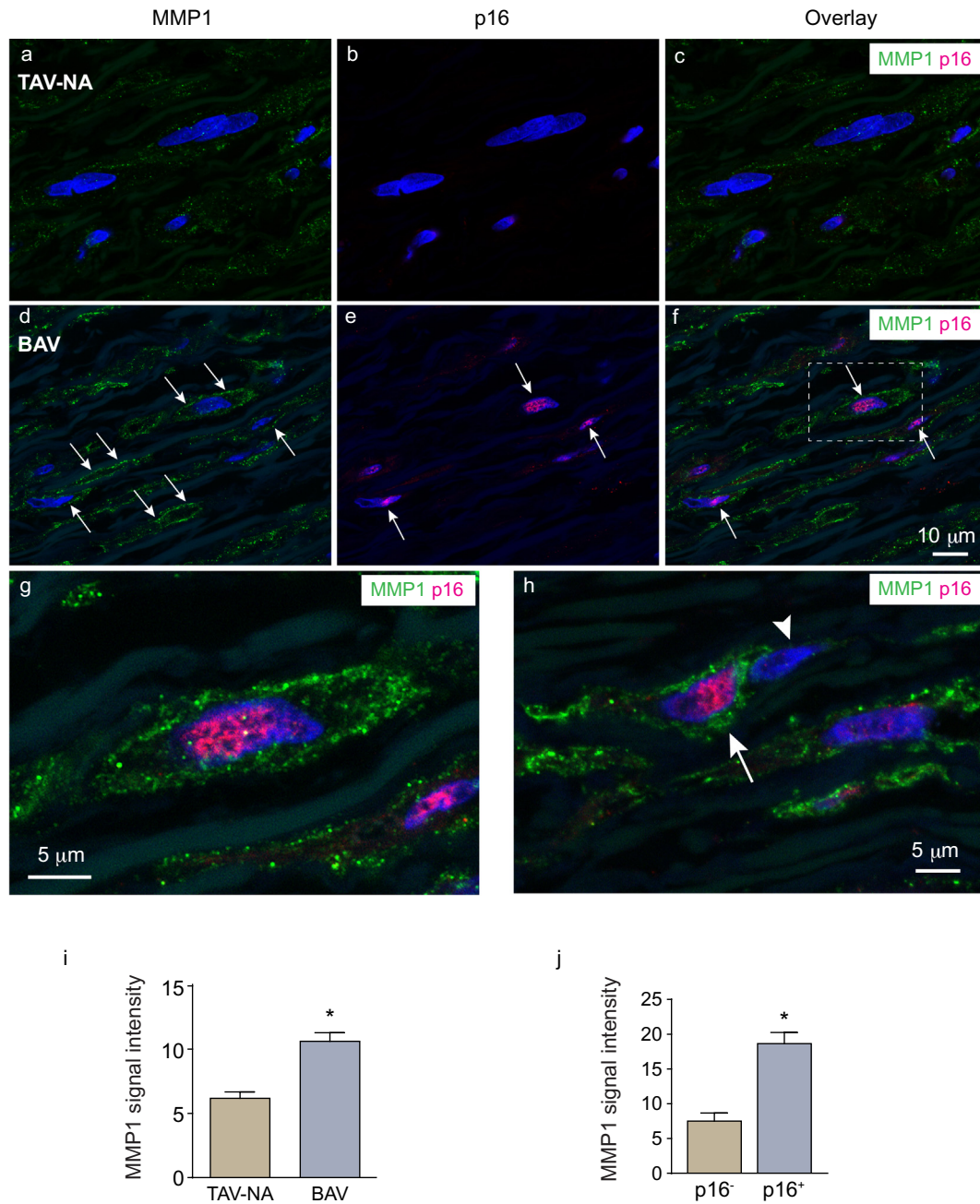


**Fig. 5.** Association of SMC senescence with the expression of MMP1. (a–h) Confocal images of human aortic sections immuno-labeled for MMP1 (green) and p16<sup>Ink4a</sup> (red) with nuclei counterstained with TO-PRO3 (blue). Cell periphery-associated MMP1 signals and p16<sup>Ink4a</sup>-positive nuclei in the BAV aorta sections (d–f) are denoted by arrows. High-magnification of the framed region in F is shown in G. In H, a p16<sup>Ink4a</sup>-positive cell with strong MMP1 signal (arrow) is adjacent to a p16<sup>Ink4a</sup>-negative cell with weak MMP1 signal (arrow head). (i) Graph depicting MMP1 signal intensity in the media of TAV-A ( $n = 7$ ) and BAV-NA/A aortas ( $n = 20$ ). \* $P = .0009$ . (j) MMP1 signal intensities of individual p16<sup>Ink4a</sup>-negative ( $n = 80$ ) and p16<sup>Ink4a</sup>-positive ( $n = 80$ ) SMCs within BAV-NA/A aortas. \* $P < .0001$ .

cell basis, light retardation by those collagen fibrils closely adjacent to p16<sup>Ink4a</sup>-positive SMCs was 43% lower than that around p16<sup>Ink4a</sup>-negative cells ( $P < .0001$ ). The pericellular collagen retardation around p16<sup>Ink4a</sup>-positive SMCs in BAV NA/A aortas was 54% lower than that around p16<sup>Ink4a</sup>-negative cells in TAV-NA aortas ( $P < .0001$ , Fig. 6e). Collectively, these findings strongly suggest that senescent SMCs in BAV aortas have degenerative consequences for collagen fibrils. In particular, there is a subset of SMCs expressing both p16<sup>Ink4a</sup> and MMP1 that have attributes of what we have termed a “seno-destructive” cell phenotype.

### 3.8. p38 MAPK regulates the collagenolytic SASP in BAV SMCs

We next asked if acquiring this seno-destructive phenotype was regulatable. p38 MAPK is a stress-activated kinase that can mediate cellular senescence [39]. As well, chronic, but not acute, activation of p38 MAPK has been identified as a driver of SASP in fibroblasts [40]. Therefore, we assessed for sustained activation of p38 MAPK in human ascending aorta by immunostaining for the phosphorylated state. This revealed discrete nuclear phospho-p38 MAPK signals in an unexpectedly high proportion of medial SMCs ( $14.0 \pm 3.6\%$ ), but with 2.8-fold

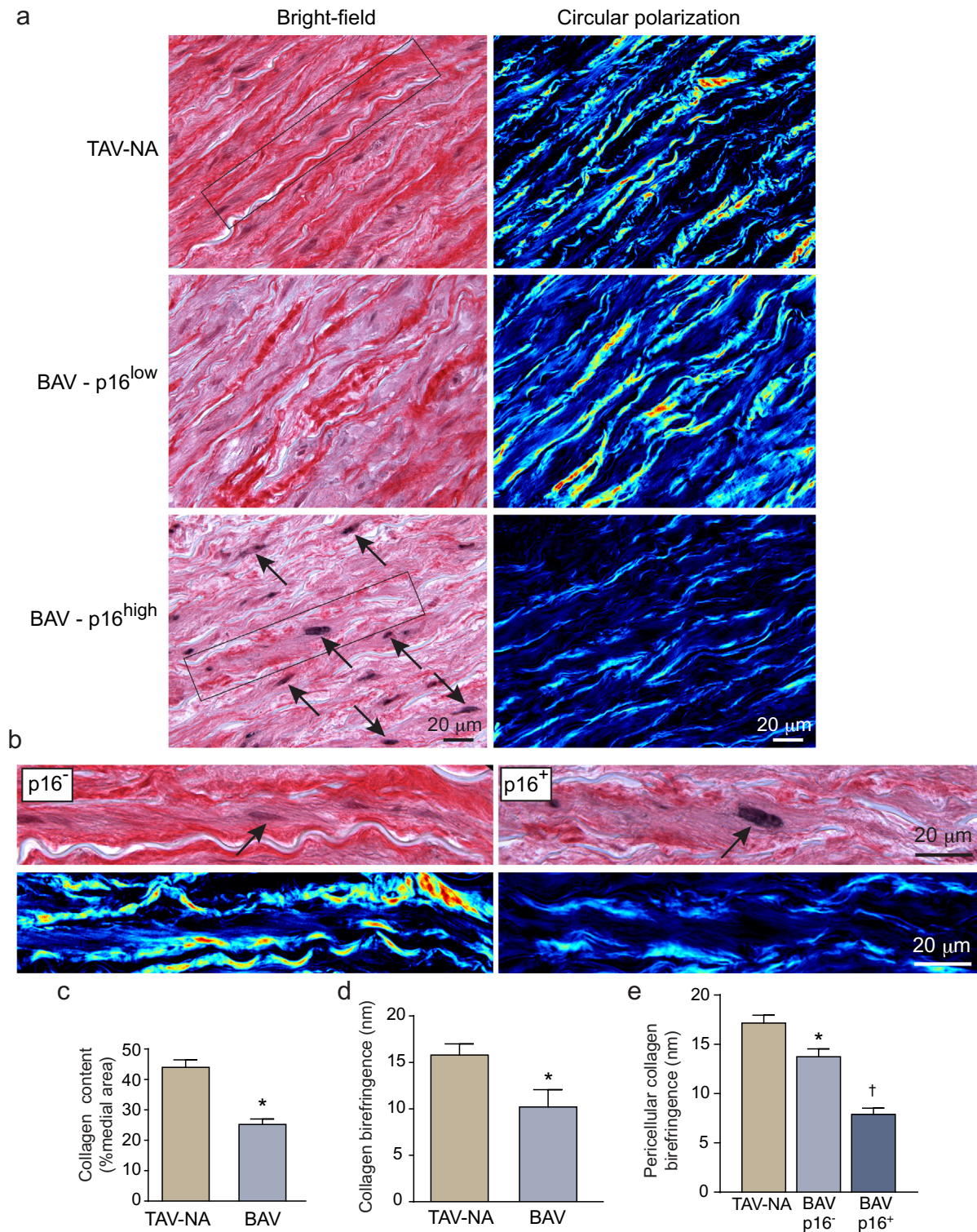


**Fig. 6.** Association of SMC senescence with collagen fibril degeneration. (a) Bright-field (left) and corresponding circular polarized light images (right) of aortic sections, dual-labeled for p16<sup>ink4a</sup> (black) and collagen fibrils (picrosirius red). The latter are imaged with circular polarization microscopy with low and high retardation signals mapped to blue and red, respectively. Depicted are sections from a control aorta (top), a region of BAV aorta with low p16<sup>ink4a</sup> signal (middle, BAV-p16<sup>low</sup>), and a region of BAV aorta with high p16<sup>ink4a</sup> signal (bottom, BAV-p16<sup>high</sup>). p16<sup>ink4a</sup>-positive medial cells are indicated by arrows. The regions with p16<sup>ink4a</sup>-negative SMCs have abundant highly-birefringent collagen fibrils. (b) Zoomed images of individual p16<sup>ink4a</sup>-negative and p16<sup>ink4a</sup>-positive SMCs (arrows) with corresponding polarization images. Thick, birefringent peri-elastin bands of collagen fibrils surround the p16<sup>ink4a</sup>-negative SMC (left), whereas thin, weakly birefringent, discontinuous fibrils surround the p16<sup>ink4a</sup>-positive SMC (right). (c) Graph depicting the collagen content in TAV-NA (n = 10) and BAV-NA/A (n = 10) aortas. \*P < .0001. (d) Collagen birefringence in TAV-NA and BAV-NA/A aortas. \*P = .036. (e) Collagen birefringence associated with individual SMCs in TAV-NA aortas (n = 38) and p16<sup>ink4a</sup>-negative (n = 31) and p16<sup>ink4a</sup>-positive SMCs (n = 33) in BAV-NA/A aortas. \*P = .037 vs. TAV-NA SMCs, †P < .0001 vs. BAV p16<sup>ink4a</sup>-negative SMCs.

more SMCs in BAV-associated aortas with p38 MAPK activation ( $P < .0001$ , Fig. 7a).

To determine if p38 MAPK signaling participated in induction of aortopathy-derived SMC senescence, cells were incubated with the specific inhibitor, SB203580. This revealed 34% and 20% reductions in p16<sup>Ink4a</sup> and p21 transcript abundance ( $P = .034$ ,  $P = .038$ ), and a 50% reduction in culture-induced SA- $\beta$ Gal-positive SMCs ( $P = .0002$ ) (Fig. 7b). Introducing p38 siRNA into BAV aortic SMCs, which decreased p38 transcript abundance by  $86.2 \pm 3.4\%$  (vs  $2.1 \pm 0.7\%$  for control siRNA), also reduced p16<sup>Ink4a</sup> and p21 expression (by 20% and 23%,  $P$

$= .004$ ,  $P = .006$ ) and the proportion of SA- $\beta$ Gal-positive SMCs (by 49%,  $P = .003$ , Fig. 7c). Importantly, inhibiting p38 in culture-aged BAV SMCs also blunted the up-regulation of MMP1 (by 47%) and MMP13 (by 71%) and reversed the upregulation MMP8 (reduced to 27% of control) (Fig. 7d). Not all SASP changes were mitigated by p38 MAPK inhibition as COL1A1 expression was unchanged ( $p = .141$ ) and the downregulated COL3A1 was modestly reduced further (10%,  $p = .007$ ). Collectively, these findings implicate p38 MAPK in the acquisition of senescence and the associated collagenolytic profile in BAV aortopathy-associated SMCs.

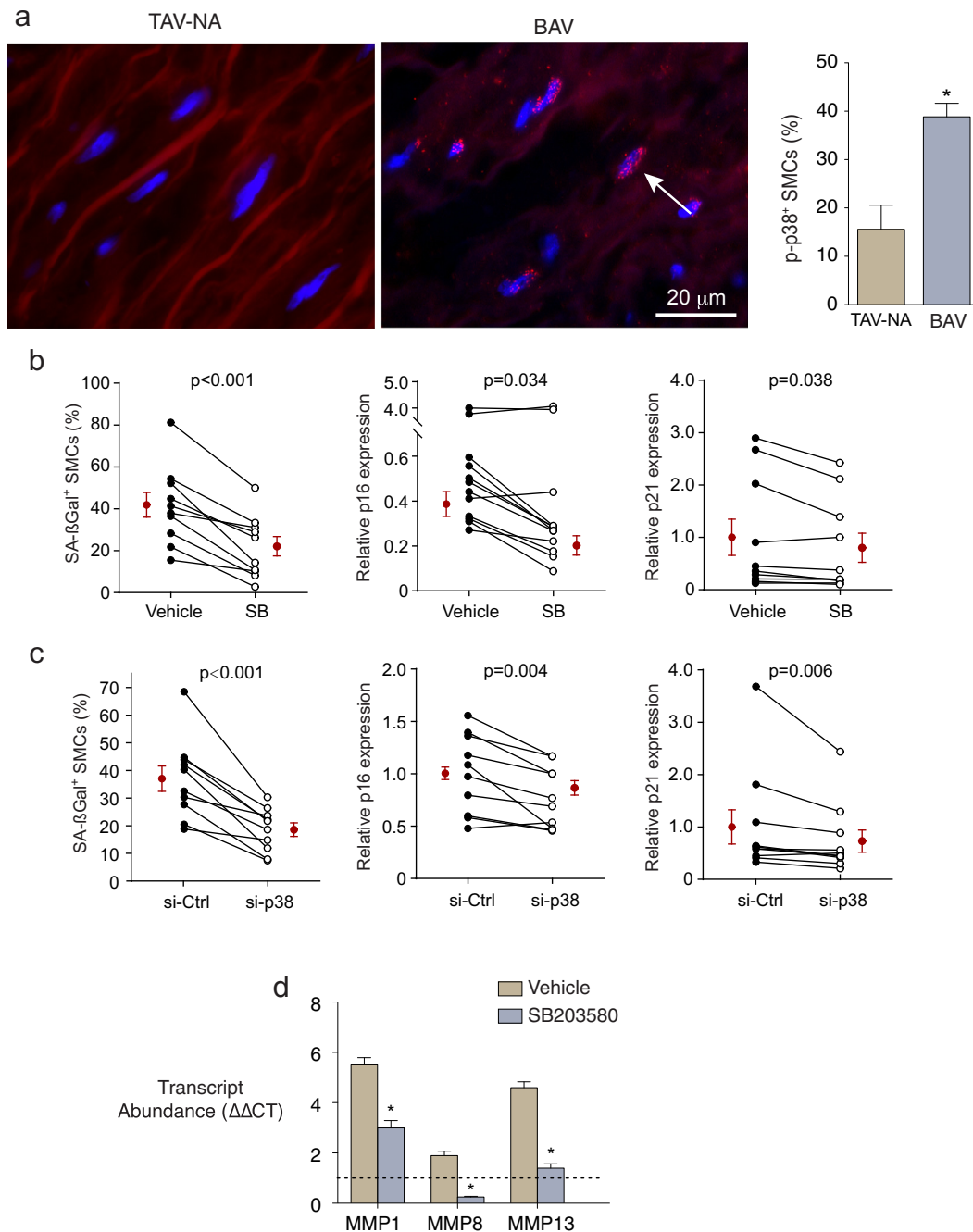


**Fig. 7.** Activation of p38 MAPK in medial SMCs in BAV aortas. (a) Fluorescence images of aorta sections immunostained for phosphorylated p38 MAPK (red nuclear foci). Nuclei were counterstained with DAPI (blue) and data are shown on right. (b-c) Graphs depicting the effect of the p38 MAPK inhibitor, SB203580 (b) or siRNA against p38 MAPK (c) on the prevalence of SMCs with SA- $\beta$ Gal activity and on transcript abundance of p16<sup>Ink4a</sup> and p21. (d) Graph depicting the effect of SB203580 on transcript abundance of MMP1, -8 and -13 in culture-aged BAV SMCs. Dashed line represents the control SMC signals set at unity. \* $P < .0001$ ,  $n = 5$ .

#### 4. Discussion

Using multiple in situ readouts we have established that: 1) ascending aortic aneurysms associated with either a bicuspid or tricuspid aortic valve contain senescent SMCs; 2) senescent SMCs are also in non-aneurysmal aortas of individuals with BAV disease, suggesting a heightened proclivity to SMC senescence in this population; 3) SMCs with unrepaired double-strand DNA breaks, a driver of senescence, are prevalent in ascending aortic disease; 4) senescent BAV SMCs have a hazardous SASP profile characterized by interstitial collagen fiber degradation; and 5) this collagenolytic phenotype is regulated by p38 MAPK signaling. These findings uncover a seno-destructive cellular cascade in ascending aortic disease, including BAV aortopathy, that could underlie its progression and the catastrophic complications.

Cellular senescence in aged tissues has the potential to be more destructive than apoptosis, the latter a SMC fate that has been recognized in ascending aortopathy for over two decades [14–16]. Unlike apoptotic cells, senescent cells can reside in tissues for extended periods, during which time they can compromise the surrounding tissue via their SASP. We found that, for aortopathy, the destructive potential of senescent SMCs was directed, at least in part, toward fibrillar collagen, the primary load-bearing element in the aorta. This senescence-collagen axis was evident by: 1) suppressed expression of  $\alpha$ -chains for types I and III collagens, the dominant collagens in the aortic media [8,41]; 2) heightened expression of those MMPs that can cleave triple helical collagen; and 3) pronounced downregulation of all four TIMPs. The observed trend toward upregulated MMP2 was also noteworthy given that increased MMP2 has been documented in BAV aortas [17,22], as has reduced TIMP1 [17,22].

In addition, we identified a population of senescent, p16<sup>Ink4a</sup>-expressing SMCs within the BAV aorta wall that strongly expressed MMP1. The MMP1 signal in these SMCs concentrated at the cell periphery, likely reflecting plasma membrane association that has been documented in cultured SMCs [42,43]. An adverse impact of p16<sup>Ink4a</sup>-MMP1-double expressing cells on aortic integrity was further supported by the finding of reduced content and birefringence of collagen fibrils adjacent to these cells. Accordingly, we propose that p16<sup>Ink4a</sup>-MMP1 double-expressing SMCs constitute hubs of degenerative activity within the ascending aorta of individuals with BAV.

That senescent SMCs were found in non-aneurysmal BAV aortas, and the multivariable statistical support for an independent association of BAV with SMC senescence, strongly suggest a predisposition of BAV SMCs for premature senescence. This is consistent with a reported proclivity of BAV SMCs for maladaptive behavior [19]. Importantly however, our findings indicate that senescence is not exclusive to BAV aneurysms. This is in keeping with a report of progerin being expressed in aneurysmal TAV aortas [18]. It is also interesting that, in BAV disease, reduced SMC differentiation and maturity have been reported [18–21] but aortic aging, a seemingly opposite paradigm, has also been proposed [31,44]. We propose that these paradigms are not mutually exclusive. Indeed, our discovery of seno-destructive SMCs in the aortic media is compatible with both scenarios, given that cellular senescence could develop from replicative stresses incurred by immature SMCs, as well as from the accumulation of oxidative and hemodynamic stresses [25]. Importantly, although our studies do not prove causality, the relationship we found between SMC senescence and aortic diameter, and the tight spatial associations among senescent SMCs, MMP1 expression, and collagen fibril attenuation, implicate SMC senescence as a determinant of the aneurysmal process itself. We propose that seno-destructive SMCs may be an early event in BAV aortopathy and also one that is exacerbated over time, in a self-perpetuating cycle of dilation and further senescence.

SMCs normally have a strong capacity to repair double strand DNA damage. The unrepaired SMC DNA lesions we observed in diseased aortas, including non-aneurysmal BAV aortas, thus indicate a vulnerability and an upstream driver of senescence. The reasons for accumulated

DNA damage signals are unknown, but it is possible that the hemodynamic disturbance arising from the BAV either directly or indirectly plays a role [45]. Such a hemodynamic linkage was supported by the observed enrichment of senescent SMCs in the aortic convexity, a region where disordered flow is concentrated [3]. We also recently identified that NAD<sup>+</sup> metabolism is perturbed in SMCs of the dilated ascending aorta, with an associated failure to repair damaged DNA [46]. We speculate that BAV aortic SMCs that are unable to effectively repair damaged DNA enter a state of senescence as a protective strategy, but that this comes at the cost of degrading the ECM through the SASP.

Fibrillar collagens are critical to the structural integrity of the aortic media, making the collagen depletion components of the SMC SASP noteworthy. However other SASP products might also contribute to aortopathy progression. For example, inhibition of stem cell-based cellular repopulation is a SASP phenomenon reported in tumors [47] and assessing the interplay between cellular senescence and cellular regeneration in the diseased aorta is warranted. Interestingly, the lack of upregulation of genes for the inflammatory cytokines/chemokines TNF- $\alpha$ , IL-1 $\beta$ , IL-6 and MIP1- $\alpha$  in senescent BAV SMCs, relative to control SMCs under the same conditions, is consistent with the non-inflammatory medial destruction of BAV aortopathy. It is thus conceivable that SMC senescence, at least in part, may explain the paradox of proteolytic damage to the aortic media with little inflammatory cell infiltrate.

We have identified sustained activation of p38 MAPK as a previously unrecognized signaling event in BAV aortopathy. Sustained activation of p38 MAPK is distinct from the more widely studied acute p38 MAPK response to stress, and has been identified as a driver of SASP in a number of cell types [39,40]. It is noteworthy therefore that expression of key collagenolytic components of the SASP profile were controlled by p38 MAPK. This finding also raises the potential for therapeutically targeting processes in the vulnerable aorta. Inhibitors of p38 MAPK are currently under investigation for therapy of a number of chronic diseases [48]. In addition, a paradigm of selective clearing of senescent cells, so-called senolytic therapy, has been proposed as a treatment strategy for aging-related diseases [49], with recent proof-of-principle human data [50]. It is interesting to consider BAV aortopathy as a potential context for senescence-targeted therapy.

In summary, we have discovered that senescent SMCs accumulate in the dilated ascending aorta of patients with BAV and TAV, and that there is a senescence predisposition in BAV aortopathy. The SASP of these prematurely aged SMCs imparts a strong collagen-depletion profile, a destructive phenotype driven by sustained activation of p38. These findings open new perspectives for managing thoracic aortopathy, including that of BAV disease.

#### Funding sources

This work was supported by the Canadian Institutes of Health Research (FRN-126148, FDN-143326) and Lawson Health Research Institute (IRF-013-09) to JGP. HY was supported by a CIHR Fellowship. JGP holds the Heart and Stroke Foundation of Ontario/Barnett-Ivey Chair. The funding sources had no involvement in the study design, collection, analysis and interpretation of data, writing of manuscript, or decision of submission.

#### Declaration of interest

M.W.A.C. has received speaker honoraria from Medtronic, Terumo Aortic, Abbott Vascular, Boston Scientific, and Cryolife.

#### Author contributions

Performed experiments: B.B., H.Y., Z.N. S.A.F., J-M.A., C.O.  
Analyzed data: B.B., H.Y., Z.N., S.R.R., S.A.F., V.K.R., J.C., J.J.L.  
Designed project, supervised recruitment, tissue procurement: M.W.A.C.

Conceived, designed, and supervised the project: J.G.P.  
Prepared the manuscript: B.B., H.Y., J.G.P.  
All authors read and approved the manuscript.

## Appendix A. Supplementary data

Supplementary data to this article can be found online at <https://doi.org/10.1016/j.ebiom.2019.04.060>.

## References

- Verma S, Siu SC. Aortic dilatation in patients with bicuspid aortic valve. *N Engl J Med* 2014;370(20):1920–9.
- Mahadevia R, Barker AJ, Schnell S, Entezari P, Kansal P, Fedak PW, et al. Bicuspid aortic cusp fusion morphology alters aortic three-dimensional outflow patterns, wall shear stress, and expression of aortopathy. *Circulation* 2014;129(6):673–82.
- Guzzardi DG, Barker AJ, van Ooij P, Malaisrie SC, Puthumana JJ, Belke DD, et al. Valve-related Hemodynamics mediate human bicuspid Aortopathy: insights from wall shear stress mapping. *J Am Coll Cardiol* 2015;66(8):892–900.
- Loscalzo ML, Goh DL, Loeyes B, Kent KC, Spevak PJ, Dietz HC. Familial thoracic aortic dilation and bicommissural aortic valve: a prospective analysis of natural history and inheritance. *Am J Med Genet A* 2007;143A(17):1960–7.
- Halushka MK, Angelini A, Bartoloni G, Basso C, Batoroewa L, Bruneval P, et al. Consensus statement on surgical pathology of the aorta from the Society for Cardiovascular Pathology and the association for European cardiovascular pathology: II. Noninflammatory degenerative diseases - nomenclature and diagnostic criteria. *Cardiovasc Pathol* 2016;25(3):247–57.
- Li S, Van Den Diepstraten C, D'Souza SJ, Chan BM, Pickering JG. Vascular smooth muscle cells orchestrate the assembly of type I collagen via alpha2beta1 integrin, RhoA, and fibronectin polymerization. *Am J Pathol* 2003;163(3):1045–56.
- Frontini MJ, O'Neil C, Sawyze C, Chan BM, Huff MW, Pickering JG. Lipid incorporation inhibits Src-dependent assembly of fibronectin and type I collagen by vascular smooth muscle cells. *Circ Res* 2009;104(7):832–41.
- Humphrey JD, Schwartz MA, Tellides G, Milewicz DM. Role of mechanotransduction in vascular biology: focus on thoracic aortic aneurysms and dissections. *Circ Res* 2015;116(8):1448–61.
- Balint B, Yin H, Chakrabarti S, Chu MW, Sims SM, Pickering JG. Collectivization of vascular smooth muscle cells via TGF-beta-Cadherin-11-dependent adhesive switching. *Arterioscler Thromb Vasc Biol* 2015;35(5):1254–64.
- Rocnik EF, Chan BM, Pickering JG. Evidence for a role of collagen synthesis in arterial smooth muscle cell migration. *J Clin Invest* 1998;101(9):1889–98.
- Zhu L, Vranckx R, Van Kien P, Khau, Lalande A, Boisset N, Mathieu F, et al. Mutations in myosin heavy chain 11 cause a syndrome associating thoracic aortic aneurysm/aortic dissection and patent ductus arteriosus. *Nat Genet* 2006;38(3):343–9.
- Guo DC, Pannu H, Tran-Fadulu V, Papke CL, Yu RK, Avidan N, et al. Mutations in smooth muscle alpha-actin (ACTA2) lead to thoracic aortic aneurysms and dissections. *Nat Genet* 2007;39(12):1488–93.
- Wang L, Guo DC, Cao J, Gong L, Kamm KE, Regalado E, et al. Mutations in myosin light chain kinase cause familial aortic dissections. *Am J Hum Genet* 2010;87(5):701–7.
- Bonderman D, Gharehbaghi-Schnell E, Wollenek G, Maurer G, Baumgartner H, Lang IM. Mechanisms underlying aortic dilatation in congenital aortic valve malformation. *Circulation* 1999;99(16):2138–43.
- Della Corte A, Quarto C, Bancone C, Castaldo C, Di Meglio F, Nurzynska D, et al. Spatiotemporal patterns of smooth muscle cell changes in ascending aortic dilatation with bicuspid and tricuspid aortic valve stenosis: focus on cell-matrix signaling. *J Thorac Cardiovasc Surg* 2008;135(1) [8–18, 18 e1–2].
- Grewal N, Franken R, Mulder BJ, Goumans MJ, Lindeman JH, Jongbloed MR, et al. Histopathology of aortic complications in bicuspid aortic valve versus Marfan syndrome: relevance for therapy? *Heart Vessels* 2016;31(5):795–806.
- Fedak PW, de Sa MP, Verma S, Nili N, Kazemian P, Butany J, et al. Vascular matrix remodeling in patients with bicuspid aortic valve malformations: implications for aortic dilatation. *J Thorac Cardiovasc Surg* 2003;126(3):797–806.
- Grewal N, Gittenberger-de Groot AC, Poelmann RE, Klautz RJ, Lindeman JH, Goumans MJ, et al. Ascending aorta dilation in association with bicuspid aortic valve: a maturation defect of the aortic wall. *J Thorac Cardiovasc Surg* 2014;148(4):1583–90.
- Grewal N, Gittenberger-de Groot AC, DeRuiter MC, Klautz RJ, Poelmann RE, Duim S, et al. Bicuspid aortic valve: phosphorylation of c-kit and downstream targets are prognostic for future aortopathy. *Eur J Cardiothorac Surg* 2014;46(5):831–9.
- Jiao J, Xiong W, Wang L, Yang J, Qiu P, Hirai H, et al. Differentiation defect in neural crest-derived smooth muscle cells in patients with aortopathy associated with bicuspid aortic valves. *EBioMedicine* 2016;10:282–90.
- Maleki S, Kjellqvist S, Paloschi V, Magne J, Branca RM, Du L, et al. Mesenchymal state of intimal cells may explain higher propensity to ascending aortic aneurysm in bicuspid aortic valves. *Sci Rep* 2016;6:35712.
- Ikonomidis JS, Ruddy JM, Benton Jr SM, Arroyo J, Brinsa TA, Stroud RE, et al. Aortic dilatation with bicuspid aortic valves: cusp fusion correlates to matrix metalloproteinases and inhibitors. *Ann Thorac Surg* 2012;93(2):457–63.
- Childs BG, Durik M, Baker DJ, van Deursen JM. Cellular senescence in aging and age-related disease: from mechanisms to therapy. *Nat Med* 2015;21(12):1424–35.
- Coppe JP, Patil CK, Rodier F, Sun Y, Munoz DP, Goldstein J, et al. Senescence-associated secretory phenotypes reveal cell-nonautonomous functions of oncogenic RAS and the p53 tumor suppressor. *PLoS Biol* 2008;6(12):2853–68.
- Yin H, Pickering JG. Cellular senescence and vascular disease: novel routes to better understanding and therapy. *Can J Cardiol* 2016;32(5):612–23.
- Shelton DN, Chang E, Whittier PS, Choi D, Funk WD. Microarray analysis of replicative senescence. *Curr Biol* 1999;9(17):939–45.
- Millis AJ, Hoyle M, McCue HM, Martini H. Differential expression of metalloproteinase and tissue inhibitor of metalloproteinase genes in aged human fibroblasts. *Exp Cell Res* 1992;201(2):373–9.
- van der Veer E, Ho C, O'Neil C, Barbosa N, Scott R, Cregan SP, et al. Extension of human cell lifespan by nicotinamide phosphoribosyltransferase. *J Biol Chem* 2007;282(15):10841–5.
- Minamino T, Yoshida T, Tateno K, Miyauchi H, Zou Y, Toko H, et al. Ras induces vascular smooth muscle cell senescence and inflammation in human atherosclerosis. *Circulation* 2003;108(18):2264–9.
- Blunder S, Messner B, Aschacher T, Zeller I, Turkcan A, Wiedemann D, et al. Characteristics of TAV- and BAV-associated thoracic aortic aneurysms—smooth muscle cell biology, expression profiling, and histological analyses. *Atherosclerosis* 2012;220(2):355–61.
- Blunder S, Messner B, Scharinger B, Doppler C, Zeller I, Zierer A, et al. Targeted gene expression analyses and immunohistochemistry suggest a pro-proliferative state in tricuspid aortic valve-, and senescence and viral infections in bicuspid aortic valve-associated thoracic aortic aneurysms. *Atherosclerosis* 2018;271:111–9.
- Hiratzka LF, Bakris GL, Beckman JA, Bersin RM, Carr VF, Casey Jr DE, et al. ACCF/AHA/AATS/ACR/ASA/SCA/SCAI/SIR/STS/SVM guidelines for the diagnosis and management of patients with thoracic aortic disease. *Circulation* 2010;121(13):e266–369.
- Roman MJ, Devereux RB, Kramer-Fox R, O'Loughlin J. Two-dimensional echocardiographic aortic root dimensions in normal children and adults. *Am J Cardiol* 1989;64(8):507–12.
- Lang RM, Badano LP, Mor-Avi V, Afilalo J, Armstrong A, Ernande L, et al. Recommendations for cardiac chamber quantification by echocardiography in adults: an update from the American Society of Echocardiography and the European Association of Cardiovascular Imaging. *J Am Soc Echocardiogr* 2015;28(1):1–39 [e14].
- Drexler M, Erbel R, Muller U, Wittlich N, Mohr-Kahaly S, Meyer J. Measurement of intracardiac dimensions and structures in normal young adult subjects by transesophageal echocardiography. *Am J Cardiol* 1990;65(22):1491–6.
- Borradaile NM, Pickering JG. Polyploidy impairs human aortic endothelial cell function and is prevented by nicotinamide phosphoribosyltransferase. *Am J Physiol Cell Physiol* 2010;298(1):C66–74.
- Ivanov A, Pawlikowski J, Manoharan I, van Tuyn J, Nelson DM, Rai TS, et al. Lysosome-mediated processing of chromatin in senescence. *J Cell Biol* 2013;202(1):129–43.
- Kurz DJ, Kloeckener-Gruissem B, Akhmedov A, Eberli FR, Buhler I, Berger W, et al. Degenerative aortic valve stenosis, but not coronary disease, is associated with shorter telomere length in the elderly. *Arterioscler Thromb Vasc Biol* 2006;26(6):e114–7.
- Iwasa H, Han J, Ishikawa F. Mitogen-activated protein kinase p38 defines the common senescence-signalling pathway. *Genes Cells* 2003;8(2):131–44.
- Freund A, Patil CK, Campisi J. p38MAPK is a novel DNA damage response-independent regulator of the senescence-associated secretory phenotype. *EMBO J* 2011;30(8):1536–48.
- McCullagh KG, Duance VC, Bishop KA. The distribution of collagen types I, III and V (AB) in normal and atherosclerotic human aorta. *J Pathol* 1980;130(1):45–55.
- Li S, Chow LH, Pickering JG. Cell surface-bound collagenase-1 and focal substrate degradation stimulate the rear release of motile vascular smooth muscle cells. *J Biol Chem* 2000;275(45):35384–92.
- Fera E, O'Neil C, Lee W, Li S, Pickering JG. Fibroblast growth factor-2 and remodeled type I collagen control membrane protrusion in human vascular smooth muscle cells: biphasic activation of Rac1. *J Biol Chem* 2004;279(34):35573–82.
- Forte A, Della Corte A. The aortic wall with bicuspid aortic valve: immature or prematurely aging? *J Thorac Cardiovasc Surg* 2014;148(5):2439–40.
- Mayr M, Hu Y, Hainaut H, Xu Q. Mechanical stress-induced DNA damage and rac-p38MAPK signal pathways mediate p53-dependent apoptosis in vascular smooth muscle cells. *FASEB J* 2002;16(11):1423–5.
- Watson A, Nong Z, Yin H, O'Neil C, Fox S, Balint B, et al. Nicotinamide phosphoribosyltransferase in smooth muscle cells maintains genome integrity, resists aortic medial degeneration, and is suppressed in human thoracic aortic aneurysm disease. *Circ Res* 2017;120(12):1889–902.
- Coppe JP, Desprez PY, Krtolica A, Campisi J. The senescence-associated secretory phenotype: the dark side of tumor suppression. *Annu Rev Pathol* 2010;5:99–118.
- Fisk M, Gajendragadkar PR, Maki-Petaja KM, Wilkinson IB, Cheriyan J. Therapeutic potential of p38 MAP kinase inhibition in the management of cardiovascular disease. *Am J Cardiovasc Drugs* 2014;14(3):155–65.
- Kirkland JL, Tchkonja T. Cellular senescence: a translational perspective. *EBioMedicine* 2017;21:21–8.
- Justice JN, Nambiar AM, Tchkonja T, LeBrasseur NK, Pascual R, Hashmi SK, et al. Senolytics in idiopathic pulmonary fibrosis: results from a first-in-human, open-label, pilot study. *EBioMedicine* 2019;40:554–63.